

Biochemical Characterization of the Diaphanous Autoregulatory Interaction in the Formin Homology Protein FHOD1*

Received for publication, August 22, 2005, and in revised form, November 17, 2005. Published, JBC Papers in Press, December 16, 2005, DOI 10.1074/jbc.M509226200

André Schönichen[‡], Michael Alexander[‡], Judith E. Gasteier[§], Fanny E. Cuesta[‡], Oliver T. Fackler[§], and Matthias Geyer^{‡1}

From the [‡]Max Planck Institute for Molecular Physiology, Department of Physical Biochemistry, D-44227 Dortmund, Germany and the [§]Department of Virology, University of Heidelberg, D-69120 Heidelberg, Germany

Diaphanous related formins (DRFs) are cytoskeleton remodeling proteins that mediate specific upstream GTPase signals to regulate cellular processes such as cytokinesis, cell polarity, and organelle motility. Previous work on the Rho-interacting DRF mDia has established that the biological activity of DRFs is regulated by an autoinhibitory interaction of a C-terminal diaphanous autoregulatory domain (DAD) with the DRF N terminus. This autoinhibition is released upon competitive binding of an activated GTPase to the N terminus of the DRF. Analyzing autoregulation of the Rac1-interacting DRF FHOD1, we utilized *in vitro* binding studies to identify a 60-amino acid DAD at the protein C terminus that recognizes an N-terminal formin homology (FH) 3 domain. Importantly, the FH3 domain of FHOD1 does not overlap with the proposed Rac1-binding domain. The FHOD1 DAD was found to contain one functional hydrophobic autoregulatory motif, while a previously uncharacterized basic cluster that is conserved in all DRF family DADs also contributed to the FH3-DAD interaction. Simultaneous mutation of both motifs efficiently released autoinhibition of FHOD1 in NIH3T3 cells resulting in the formation of actin stress fibers and increased serum response element transcription. A second putative hydrophobic autoregulatory motif N-terminal of the DAD belongs to a unique FHOD subdomain of yet undefined function. NMR structural analysis and size exclusion chromatography experiments revealed that the FHOD1 DAD is intrinsically unstructured with a tendency for a helical conformation in the hydrophobic autoregulation motif. Together, these data suggest that in FHOD1, DAD acts as signal sequence for binding to the well folded and monomeric FH3 domain and imply an activation mechanism that differs from competitive binding of Rac1 and DAD to one interaction site.

Formin proteins are involved in the regulation of many cytoskeletal processes including cytokinesis, actin cable and stress fiber formation, polarity establishment, neurite outgrowth, and intracellular trafficking (reviewed in Refs. 1 and 2). These functions are achieved by their ability to promote F-actin assembly at the filament barbed end and to move processively with the barbed end as it elongates (3–7). Formins are large proteins of typically more than 1000 amino acids that are defined by the presence of two conserved regions, namely the formin homology 1 and

2 (FH1 and FH2)² domains (1). Additional conserved domains such as a N-terminal GTPase-binding domain (GBD) and a C-terminal diaphanous autoregulation domain (DAD) were found to constitute a formin subfamily, the diaphanous related formins (DRFs) (8). Over the last years, DRFs have emerged as a group of proteins with the potential to bridge between G-protein signals and the cytoskeleton via their ability to bind activated small GTPases and to subsequently remodel the cytoskeleton (9–13).

At present, phylogenetic analyses of FH2 domains suggest that metazoan formins fall into seven groups, termed Dia (diaphanous), DAAM (dishevelled-associated activator of morphogenesis), FRL (formin-related gene in leukocytes), FHOD (formin homology domain-containing protein), INF (inverted formin), FMN (formin), and delphilin (14). FHOD1 (previously named FHOS) was initially identified in splenic cells as an interaction partner of the acute myeloid leukemia transcription factor (AML-1B) (15). It is ubiquitously expressed and facilitates transcription from the serum response element (SRE) (15, 16). An activated form of FHOD1 in which autoinhibition is constitutively released induces the formation of and association with actin stress fibers (16–18). FHOD1 was shown to stimulate cell migration in an integrin-independent manner (18), an effect that may relate to its ability to coordinate actin filaments and microtubules to induce cell elongation (19). A recently identified homolog, FHOD2, is expressed in heart, kidney, and brain and localizes to nestin intermediate filaments to promote their actin-organizing activity (20).

The biological activity of DRFs is mediated by its central FH1-FH2 module that nucleates actin filaments and remains bound to the barbed end of the growing filament (21–23). Structural analyses have provided the molecular basis of a tethered dimer architecture that may allow formins to stair-step on the barbed end of an elongating nascent filament by binding two actins, one permitting monomer binding and the other permitting monomer dissociation (24–26). However, in context of the full-length proteins, DRF molecules are thought to exist in an inactive state due to an intramolecular interaction between the C-terminal autoregulatory DAD and its N-terminal recognition domain (8, 27–29). This interaction requires a regulatory motif (MDxLL) in the DAD (8) and is suggested to mask the conserved FH1 and FH2 domains, thereby autoinhibiting their biological activity. DRF-DADs also contain a highly conserved cluster of positively charged residues with yet unknown relevance to autoregulation (8). This autoinhibition is

* This work was supported by a fellowship from the Chica and Heinz Schaller Stiftung (to O. T. F.). The costs of publication of this article were defrayed in part by the payment of page charges. This article must therefore be hereby marked "advertisement" in accordance with 18 U.S.C. Section 1734 solely to indicate this fact.

¹ To whom correspondence should be addressed: Max-Planck-Institut für Molekulare Physiologie, Abt. Physikalische Biochemie, Otto-Hahn-Str. 11, 44227 Dortmund, Germany. Tel.: 49-231-133-2366; Fax: 49-231-133-2399; E-mail: matthias.geyer@mpi-dortmund.mpg.de.

² The abbreviations used are: FH, formin homology; DAD, diaphanous autoregulatory domain; DRF, diaphanous-related formin; FHOD1, formin homology 2 domain-containing protein 1; GBD, GTPase-binding domain; GST, glutathione S-transferase; HA, hemagglutinin; ITC, isothermal titration calorimetry; SRE, serum response element; TRITC, tetramethylrhodamine isothiocyanate; TCEP, Tris(2-carboxyethyl)phosphine hydrochloride.

released upon interaction with specific members of the Rho-family GTPases in their activated state (8, 28). Consequently, DRF proteins lacking the DAD or its recognition domain behave as dominant active molecules with substantial actin remodeling activity (8, 13, 16, 27, 30). Recent structural data have shed light on the activation interaction for the mDia1 protein (31, 32). The structurally and functionally less well defined FH3 domain (33), also referred to as diaphanous inhibitory domain (29), was found to interact with the autoregulating DAD (32), while a small preceding region forms the GTPase-binding subdomain of mDia1 that interacts with the switch I and II regions of the Rho GTPase (31). A succeeding three-helix bundle forms a dimerization domain, which is believed to be followed by a coiled-coil region before the proline-rich FH1 domain starts.

Several lines of evidence suggest that the molecular mechanisms of autoinhibition for FHOD formins could differ from that of Dia-family formins. First, although the N-terminal regions of mDia1 and FHOD1 are of similar length, there is no apparent homology between the two different subfamily proteins (16.7% identity over 570 residues). In fact, the overall modular domain architecture of FHOD1 and mDia1 seems to be distinct, since the GTP-binding region was suggested to directly precede the FH1 domain in FHOD1 (Ref. 16; see also Fig. 1A) while it was mapped to a near N-terminal domain in mDia1 (27–29, 31, 32). Moreover, FHOD family proteins interact with Rac1 instead of Rho or CDC42 GTPases (16, 17). In contrast to the mDia-GTPase interaction, binding of FHOD1 to Rac1 is not regulated by the loaded nucleotide state of the GTPase and activated Rac1 fails to induce the full phenotype observed with dominant active FHOD1 (16, 17). Finally, also the C-terminal DAD in FHOD1 differs from Dia family DADs by its length and the number of potential autoregulation signals (Fig. 1, B and C). This leads to an ambiguous alignment between these DADs. While current listings (e.g. SMART) provide a lineup with no gaps between the FH2 and DAD, an alternative alignment scheme might assemble the C-terminal motifs for functional similarities (Fig. 1D, left and right panels).

This study focused on the biochemical analysis of the autoregulation within human FHOD1. We found that an N-terminal stable domain (FH3, 1–377) directly interacted with the DAD. Mutation of the three proposed DAD consensus motifs showed that only the two C-terminal motifs contributed to FH3 domain binding *in vitro* and control FHOD1 activity in cells. Structural analysis of the FHOD1 DAD revealed an intrinsically unstructured domain with some tendency for a helical conformation in the hydrophobic consensus motif. The DAD could act as signal sequence for binding to the well folded and monomeric FH3 domain. These data imply that distinct, individually adapted molecular surfaces mediate the autoregulation and activation mechanism of FHOD1 that contains an additional region in between the FH2 domain and DAD.

EXPERIMENTAL PROCEDURES

Protein Sequence Analysis—Sequence alignments and protein secondary structure predictions were done prior to protein fragmentation using following protein sequence data base entries: FHOD1 (human) Q9Y613, FHOD1 (mouse) AAH60654, FHOD2 (mouse) BAC98303, FHOD3 (human) XP_371114, mDia1 (mouse) O08808, DRF1/hDia1 (human) O60610, mDia3 (mouse) O70566, DRF2/hDia2 (human) O60879, diaphanous (*Drosophila*) P48608, DRF3/mDia2 (mouse) Q9Z207, and Bni1p (yeast) P41832. Multiple sequence alignments were performed using the MultAlign software (au.expasy.org/). For domain architecture analyses and secondary structure predictions following open access programs were quoted: SMART (smart.embl-

heidelberg.de/), Prosite (au.expasy.org/prosite/), and PredictProtein (www.predictprotein.org/).

Plasmid Cloning, Protein Expression, and Purification—The coding DNA sequence for human *fhod1* (GenBank™ accession code: AF113615) was used to generate fragments thereof by PCR-mediated amplification with primer containing BamHI and EcoRI restriction sites at the 5′- and 3′-ends, respectively. Fragments were cloned in the prokaryotic expression vectors pProEx-HTb (Invitrogen) or pGEX-2T-tev (Amersham Biosciences) for protein expression and purification. Codon optimization of the DAD was performed using the mega-primer method for mutagenesis as described previously (34). Site-directed mutagenesis of DAD consensus motifs was conducted similarly using both sense and antisense oligo nucleotides. Full-length plasmids for cellular transfection assays were cloned in the pEF-HA vector similarly as described (17), which contained an N-terminal HA-epitope for immunostaining.

For expression of FHOD1 protein domains the coding plasmids were transformed into *Escherichia coli* BL21(DE3) cells (Novagen), expressed at 30 °C and induced at an A_{600} of 0.6 to 1.0 with 0.3 mM IPTG for 5 h growth. For His-tagged proteins cells were fluidized in lysis buffer A (20 mM Tris/HCl, pH 7.6, 500 mM NaCl, 5 mM β -mercaptoethanol) with 20 mM imidazole and cleared by spinning for 45 min at 30,000 $\times g$. The lysate was loaded onto 5 ml of nickel-nitrilotriacetic acid resin (Qiagen) that had been pre-equilibrated with lysis buffer. After washing with 10 volumes of lysis buffer A the protein was eluted with 10 volumes of lysis buffer A using a linear gradient from 20 to 250 mM imidazole. The peak fractions were dialyzed in buffer A, and if required the histidine tag was cleaved off at 4 °C over 12 h with Tev protease. FHOD1 was depleted of the protease and of uncleaved fragments by affinity chromatography. The protein containing flow-through was concentrated and further purified by gel filtration on a S75 column in 20 mM Tris/HCl, pH 7.6, 150 mM NaCl. GST fusion proteins (377–573 and 1104–1164) were expressed as described above and fluidized in 20 mM Tris, 150 mM NaCl, 1 mM EDTA, pH 8.0. After washing with 20 mM Tris/HCl, 1 M NaCl, 1 mM EDTA GST fusion proteins were eluted with 10 mM GSH and cleaved by Tev-protease at 4 °C over 12 h. GSH was removed by gel filtration and GST by GSH affinity column. Uniformly ^{15}N -labeled DAD of FHOD1 was produced in minimal medium containing $^{15}\text{NH}_4\text{Cl}$ as the sole nitrogen source. Fractions were analyzed by SDS-PAGE and fractions containing FHOD1 proteins (about 98% pure) were concentrated (Amicon filter) and stored at -80°C . Protein concentrations were determined by Bradford assay (Bio-Rad) and extinction coefficient measurements.

GST Pull-down Assays and Western Blotting—For direct interaction assays between various DAD constructs and the N-terminal domains of FHOD1 (1–573), the FH3 domain (1–377), and the proposed GBD domain (377–573), about 2 μg of GST or GST fusion proteins were immobilized on glutathione-Sepharose beads (Amersham Biosciences) and incubated with 10–20 μg of the respective target protein. Binding reactions were performed in 500 μl of buffer solution (20 mM Tris/HCl, pH 7.6, 150 mM NaCl, 1 mM dithioerythritol, 0.1% Nonidet P-40) for 1–3 h at 4 °C or for 0.5 h at room temperature, respectively. Beads were washed three to five times in the same buffer, and bound proteins were analyzed by SDS-PAGE and subsequent Coomassie staining or Western blotting, respectively, using standard protocols. Recombinant proteins were detected with an anti-His antibody (Santa Cruz Biotechnology). Expression of HA-tagged FHOD1 proteins in transfected NIH3T3 cells was analyzed by SDS-PAGE/Western blotting of postnuclear cell lysates with an anti-HA antibody (Santa Cruz Biotechnology).

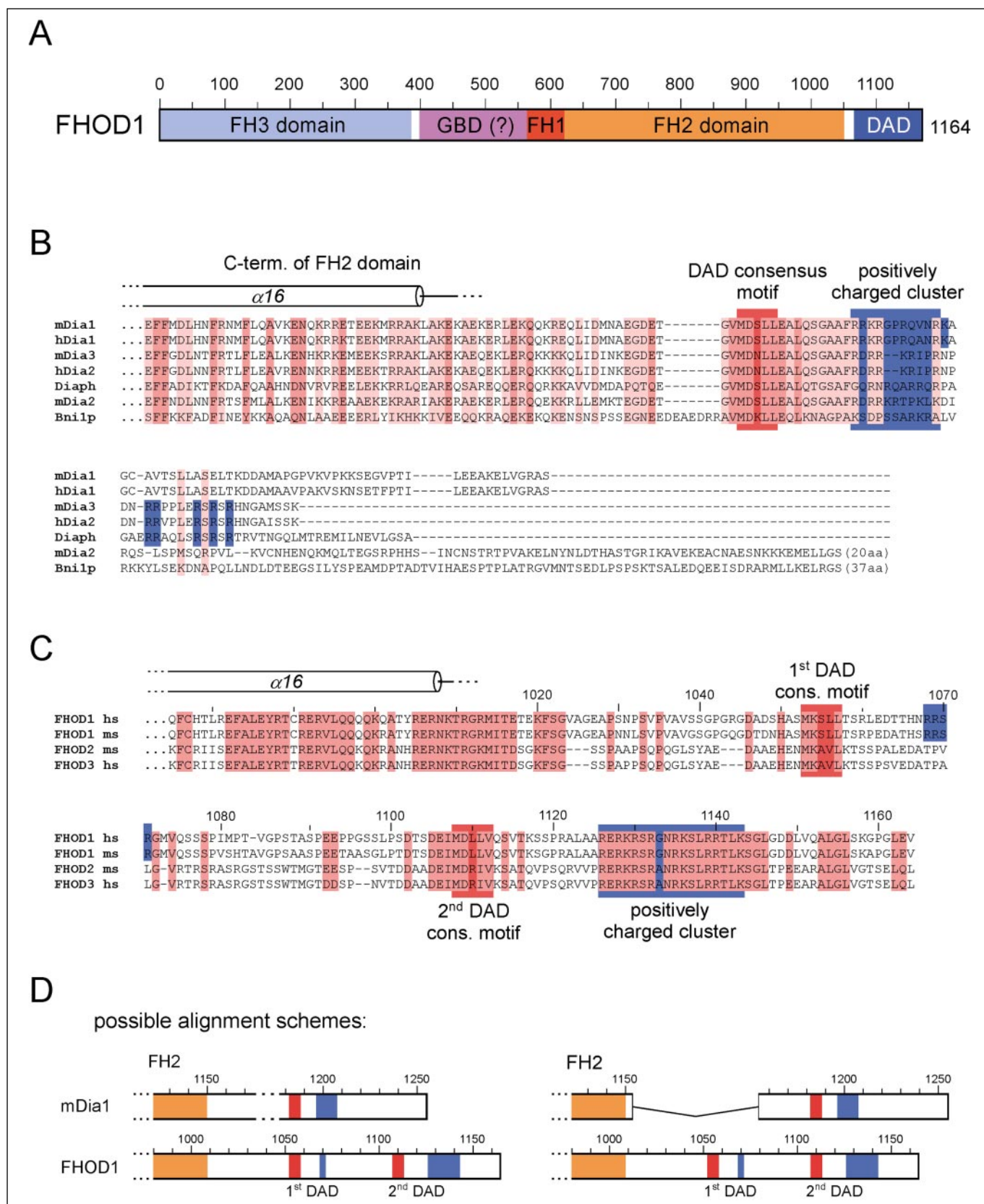


FIGURE 1. **Modular domain composition of FHOD1 and sequence alignment of diaphanous autoregulatory domains.** A, proposed domain arrangement of human FHOD1 (GenBank™ accession code: Q9Y613) including the N-terminal FH3 domain (also named DID), the GBD, the proline-rich FH1 domain, the central FH2 domain that mediates actin nucleation, and the C-terminal DAD. B and C, alignment of DAD sequences from diaphanous-related formins. B, the Dia family formins contain one DAD consensus motif (MDxLL) and a succeeding positive cluster of at least seven positively charged residues. The C-terminal helix of the FH2 domain as derived from crystal structures (24–26) is indicated on top. C, in contrast, FHOD family proteins contain two potential DAD consensus motifs at positions 1053 (MKxLV) and 1108 (MDxLV) and a positively charged cluster of 18 residues length at position 1126 that contains 10 positively charged residues. D, Possible alignment schemes for Dia and FHOD family formins. While current listings provide a lineup with no gaps between the FH2 and DAD (left-hand side), an alternative alignment scheme might assemble the C-terminal motifs for functional similarities (right-hand side).

Transfections and Immunofluorescence Microscopy—Functional analyses of FHOD1 proteins were carried out in NIH3T3 cells essentially as described previously (17). For immunofluorescence, cells were plated onto coverglasses overnight and subsequently transfected with a total of 1 μg of DNA using Metafectene (Biontex). 24 h post-transfection, the cells were fixed with 3% paraformaldehyde (15 min at room temperature), permeabilized with phosphate-buffered saline, 0.1% Triton X-100 for 2 min, and blocked with phosphate-buffered saline, 1% bovine serum albumin for 30 min. HA-tagged FHOD1 proteins were revealed by staining with the mouse monoclonal antibody F-7 (Santa Cruz Biotechnology) and appropriate secondary antibodies conjugated with Alexa 488 (Molecular Probes). F-actin was stained with TRITC-conjugated phalloidin (Sigma). Following extensive washing, cells were mounted with Histogel (Linaris), and indirect fluorescence images were monitored with an Olympus IX70 microscope and processed using Adobe Photoshop.

SRE Transcription Assay—Activation of the SRE by FHOD1 was quantified in NIH3T3 cells as described previously (17). Briefly, luciferase activity of NIH3T3 cells was determined 24 h post-transfection of FHOD1 expression vectors, the 5 \times SRE-Luc reporter plasmid, and pTK-*Renilla* with a Luminoskan Ascent luminometer (Thermo Laboratories) using the dual luciferase reporter assay system kit (Promega). SRE firefly luciferase counts were normalized to the activity of the *Renilla* luciferase internal control and calculated as fold transactivation with the counts for FHOD1-wt arbitrarily set to 1.

Isothermal Titration Calorimetry—The thermodynamic parameters of the FHOD1 interaction with wild type and mutant DAD were determined by isothermal titration calorimetry (MCS-ITC, MicroCal). All proteins were dialyzed against ITC buffer (50 mM Hepes, pH 7.2, 100 mM NaCl, 1 mM TCEP), and the DAD fragment (1104–1164) was thermostated in the sample cell at 25 $^{\circ}\text{C}$ at a concentration of 35 μM . The FH3 domain-containing fragment (400 μM) was injected stepwise by volumes of 8 μl from the syringe into the solution. The change in heating power was observed for 4 min until equilibrium was reached before the next injection was started. Further data evaluation was performed using the manufacturers analysis software, yielding ΔG° and ΔH° values with 0.5 kcal/mol errors each and typical errors for dissociation constants of 0.5 μM and somewhat higher for weak binding mutants.

Analytical Gel Filtration Chromatography—Analytical gel filtration experiments were performed with a multicomponent Waters 626 LC system (Waters) using a Superdex 75 column (10/30, column volume 25.7 ml, Amersham Biosciences) or a Biosep-SEC-S2000 column (300 \times 1.8 mm, Phenomenex) with a separation range for globular proteins from 1 to 300 kDa. The columns were first equilibrated in the respective running puffer following injection of the protein samples. The flow rate was set to 0.5 or 1.0 ml/min for the Superdex or Biosep column, respectively. Elution profiles were monitored by UV absorption at 280 nm. The void volume (V_0) was determined with blue dextran (Sigma). The columns were calibrated with the following standards (Bio-Rad): thyroglobulin (670 kDa), bovine γ -globulin (158 kDa), chicken ovalbumin (44 kDa), equine myoglobin (17 kDa), and vitamin B₁₂ (1.35 kDa). The ratio of elution volume to void volume (V_e/V_0) was plotted *versus* the $\log(M_r)$ for each standard to generate a linear calibration curve. FHOD1 samples were dialyzed from frozen stocks into the equilibration buffer, diluted to a concentration of 1 mg/ml each, and injected onto the column at a volume of 90 μl . Protein complexations were incubated for 30 min prior to subjection to the column. The apparent molecular weight of each FHOD1 fragment was determined from the standard curve. Gel filtration experiments were performed repeated times at room temperature.

NMR Spectroscopy—NMR experiments with homonuclear or ¹⁵N-labeled protein samples were performed on a Varian Inova 600 spectrometer, equipped with a triple resonance probe with shielded Z gradients. Proteins were dissolved in phosphate buffer (20 mM KP_i, pH 7.0, 100 mM NaCl, 1 mM TCEP) at a concentration of 0.6 mM and measured at 25 $^{\circ}\text{C}$ in SHIGEMI tubes. Homonuclear two-dimensional experiments and ¹⁵N/¹H-heteronuclear HSQC experiments were recorded following the Varian NMR suite with typically 2048 \times 512 data points. NMR spectra were converted to Bruker format and processed with XWINNMR and evaluated and plotted with Aurelia (35). The assignment strategy was based on the identification of individual resonance spin systems from homonuclear TOCSY experiments following the sequential path with homonuclear two-dimensional and ¹⁵N-separated three-dimensional NOESY spectra similarly are described (36).

RESULTS

Identification of the Diaphanous Autoregulatory Domain in FHOD1 and Its Interacting Domain—We started to analyze the domain boundaries of the interacting C-terminal DAD and its N-terminal recognition domain by GST pull-down binding assays. To this end we first expressed a construct in *Escherichia coli* bacterial cells that started C-terminal to the proposed FH2 domain at position 1032 and went up to the C terminus of the protein (Fig. 2A, left lane). Analytical mass spectrometry, however, revealed a proteolytic cleavage or premature truncation of the fragment that corresponded to an apparent mass of 10,046 Da (data not shown). This termination corresponded to the second appearance of a rare AGG codon at amino acid position 1126, which encoded the first arginine residue of the positively charged cluster of the DAD (Fig. 1C). Expression in BL21-CodonPlus(DE3)-RIL cells (Stratagene) that carry extra copies of the *argU*, *ileY*, and *leuW* tRNA genes still did not result in homogeneous protein expression (Fig. 2A, middle lane). We therefore introduced silent mutations of four rare codons, AGG, AGA, and CTC at positions 1060, 1139, 1140, and 1146, respectively, to more commonly used codons which finally yielded full-length expression of the DAD (Fig. 2A, right lane). Of note, the GST fusion construct contained a linker segment with two individual sites for thrombin and Tev protease cleavage resulting in the appearance of two GST protein bands at 27 and 30 kDa.

As described in the introduction section the modular domain composition of the N terminus of FHOD1 (1–573) that is preceding the FH1 and FH2 domain cannot be deduced from results of recent studies on the mDia family proteins. A direct sequence alignment of the N-terminal regions, *e.g.* between mDia1 and FHOD1 proteins, resulted in an identity of 16.7% although both sequences were of similar length with 572 and 570 residues, respectively. Moreover, the GTPase-binding domain, which encompasses residues (75–260) in mDia1 (27, 29, 31, 32), is proposed to be in between amino acids 422 and 717 in FHOD1 (16). However, sequence alignments of mutually swapped fragments again did not show any significant homologies that would be predicted to result in similar folds. Therefore, we further dissected the N-terminal FHOD1 fragment based on secondary structure predictions and generated the two fragments (1–377 and 377–573) (Fig. 2A, right panel). Both protein fragments were soluble and stable and could be purified using standard techniques. We expressed the codon optimized DAD fragment (1032–1164) fused to GST and tested binding with His-tagged N-terminal domains from precipitations by subjection to SDS-PAGE and blotting with anti-His antibody. While the two N-terminal fragments (1–573 and 1–377) bound to the DAD, the proposed GBD fragment (377–573) did not (Fig. 2B). Since binding of 1–377 was more robust than that of 1–573, the shorter fragment represents an optimized

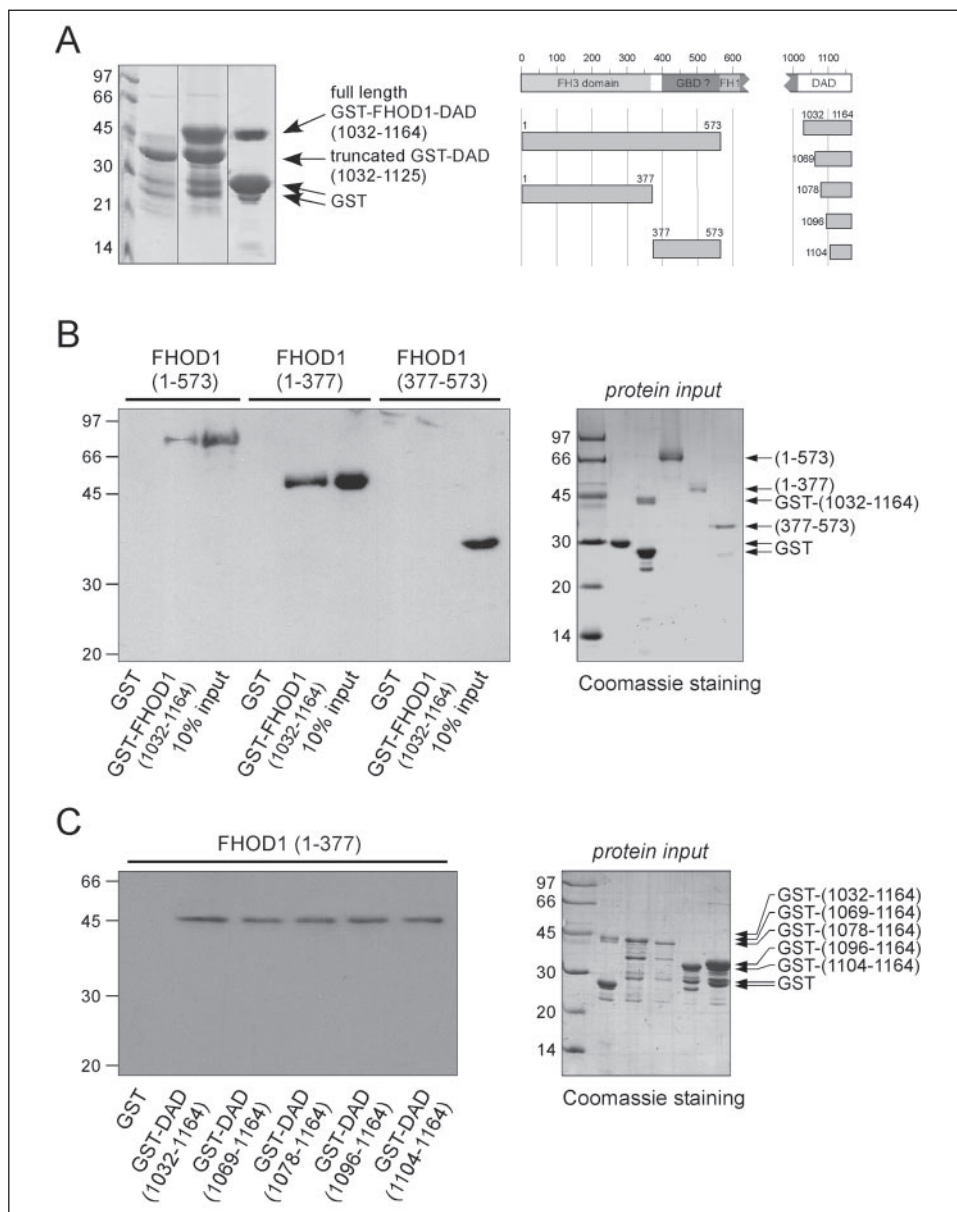


FIGURE 2. The C-terminal 60 residues of the DAD are essential for binding to the N-terminal domain of FHOD1. *A*, codon optimization led to expression of the full-length GST-FHOD1-DAD protein (1032–1164). Expression of the GST-DAD in BL21(DE3) cells led to a truncation at the first arginine (1126) of the positively charged cluster (*left lane*). Expression in BL21(DE3)-RIL cells yielded both full-length and truncated GST-DAD fusion protein (*middle lane*), while only codon optimization resulted in the full-length protein (*right lane*). A schematic of the proteins used is shown in the *right panel*. *B*, the DAD binds the N-terminal domain (1–377) of FHOD1 but not the proposed GBD (377–573). Western blot of a GST pull-down experiment with GST-fused FHOD1-DAD and three N-terminal fragments of FHOD1 (1–573, 1–377, and 377–573) that contain a hexahistidine epitope. The proteins used are shown in the *right panel*. *C*, the DAD of FHOD1 encompasses residues 1104–1164. N-terminal truncations of the DAD in five steps from position 1032 to 1104 revealed that the smallest fragment (1104–1164) is sufficient for binding to the N-terminal domain. The protein input used in this experiment is shown in the *right panel*.

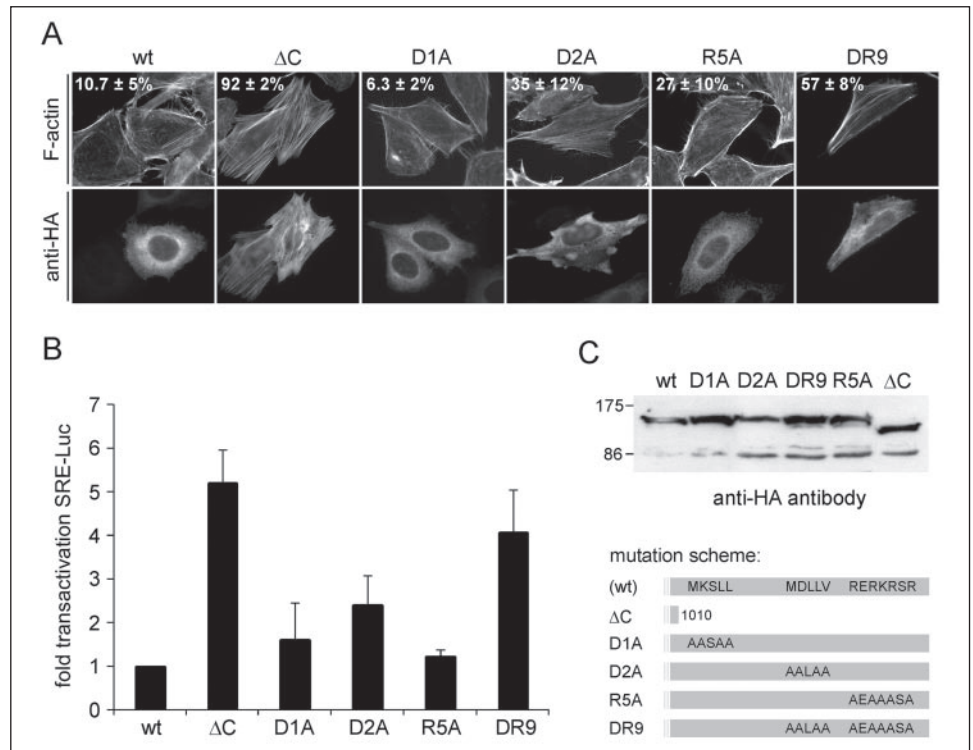
interaction domain of the FHOD1 DAD. In the initial publication, the FH3 domain was recognized as a repetitive region (33), which later turned out to bind the DAD in mDia1 (8, 27, 32). We therefore considered the fragment 1–377 as FH3 domain of FHOD1.

Next we wanted to narrow down the minimal DAD fragment that is required for FH3 domain binding. Five different fragments ranging from 1032–1164 to 1104–1164 were cloned based on the codon optimized plasmid, expressed in *E. coli* and purified. They all showed similar binding properties to the N-terminal recognition domain, suggesting that the shortest fragment which starts four residues prior to the second DAD consensus motif in FHOD1 (Fig. 1C) is still sufficient for FH3 domain binding. Of note, a DAD construct (1012–1164) that directly started after the proposed C-terminal helix of the FH2 domain was insoluble and could not be purified (data not shown). We conclude that the C-terminal 60 residues of FHOD1 compose the DAD domain that interacts with its recognition domain (1–377).

Role of the DAD Consensus Motifs for the Biological Activity of FHOD1 in NIH3T3 Cells—To search for amino acids within the DAD of FHOD1 involved in autoinhibition of the DRF, we aligned the C-terminal

sequences of the known mouse and human FHOD family members (Fig. 1C) and various other DRFs (Fig. 1B). This analysis revealed that FHOD proteins contain two putative autoregulatory MDxLL motifs and one positively charged cluster, while other DRF DADs only contain one copy of each motif. To address the individual contribution of these motifs for the autoregulation of FHOD1 in cells, we generated mutants of the three DAD consensus signals and one combined double mutation in the mammalian expression plasmid for full-length HA-tagged FHOD1 (see Fig. 3C, lower panel). First, the two potential hydrophobic autoregulatory motifs present in the FHOD1 DAD were changed, MKSLL at position 1053 to AASAA (named D1A) and MDLLV at position 1108 to AALAA (named D2A). We also mutated the conserved positively charged cluster RERKRSR at position 1126 to AEAASA (named R5A). Finally, we combined the mutation of the second DAD consensus motif (D2A) with the mutation of the charged cluster (R5A) to generate the double mutant DR9. All these constructs expressed stable proteins of the expected size to levels comparable with those of wild type FHOD1 (FHOD1-wt) and its ΔC variant (1–1010) lacking the last 154 amino acids when transfected into NIH3T3 cells (Fig. 3C, upper

FIGURE 3. Simultaneous mutation of the MDxLV motif and the basic cluster in the DAD releases the intramolecular autoinhibition of FHOD1 and triggers its activation in cells. *A*, subcellular localization and effects on the actin cytoskeleton of the various FHOD1 mutants. NIH3T3 cells were transfected with the indicated FHOD1 expression plasmids. Following fixation, the cells were stained for F-actin (upper panel) and HA-FHOD1 (lower panel) and analyzed by immunofluorescence microscopy. The numbers indicate the mean percentage with S.D. of cells expressing the respective FHOD1 variant that displayed thick actin stress fibers in three independent experiments with at least 100 cells evaluated each. Since stress fibers induced by FHOD1-D2A appeared to be less bundled, the respective number for this FHOD1 variant refers to cells that display elevated levels of thin actin stress fibers. *B*, SRE luciferase reporter assay. Shown are fold transactivation of the SRE luciferase reporter in NIH3T3 cells expressing the indicated FHOD1 variants. Luciferase activity for FHOD1-wt expressing cells was arbitrarily set to 1. Presented are average values from at least three independent experiments with the indicated standard error of the mean. *C*, Western blot analysis of the cells used in *A* and *B* (upper panel). 2×10^5 NIH3T3 cells transfected with the indicated FHOD1 expression plasmids were resolved by SDS-PAGE and analyzed after Western blotting with an anti-HA antibody. The lower panel depicts a schematic representation of the FHOD1 variants analyzed.



panel). FHOD1 variants lacking the C terminus including the DAD are thought to be constitutively active, which is reflected in their ability to trigger the formation of thick actin stress fibers and to activate transcription from the SRE (16–18, 37). We thus made use of these biological readouts to determine the role of the individual motifs in the FHOD1 DAD for autoinhibition in cells.

Expectedly, FHOD1-wt was found throughout the cytoplasm of transfected NIH3T3 cells and did not induce significant changes in F-actin organization (Fig. 3A). In contrast, FHOD1- ΔC caused the formation of thick actin stress fibers and co-localized with these structures. While the D1A FHOD1 variant was virtually indistinguishable from FHOD1-wt in this analysis, the R5A, D2A, and DR9 FHOD1 mutants caused the formation of actin stress fibers in NIH3T3 cells. This effect was most pronounced for FHOD1-DR9, which triggered formation of thick stress fiber bundles in $57 \pm 8\%$ of transfected cells; however, the number of these structures per cells was reduced relative to FHOD1- ΔC expressing cells. In contrast, the FHOD1 R5A and D2A variants were active only in a relatively small fraction of the cells ($27 \pm 10\%$ and $35 \pm 12\%$, respectively) and induced stress fibers that were markedly thinner than those induced by other activated FHOD1 variants. Notably, FHOD1-DR9 caused formation of thick actin stress fibers despite the lack of apparent association of the DRF with these filaments. Similar results were obtained when the effects of the various FHOD1 proteins on transcription of the SRE were examined (Fig. 3B). FHOD1- ΔC induced an approximately 5-fold activation, while FHOD1-D1A and R5A were inactive in this assay. FHOD1-D2A caused a weak induction of SRE transcription, and the DR9 FHOD1 variant was almost as active as FHOD1- ΔC . Together, these results indicate that the MDLLV motif and the positively charged cluster are determinants for autoregulatory interactions of the FHOD1-DAD in cells and that simultaneous disruption of both interaction sites triggers the biological activity of the DRF.

The MDxLV Motif Is Required for Autoinhibition—To further analyze the contributions of the individual DAD consensus motifs to the interaction with the FH3 domain by biochemical means we performed

isothermal titration calorimetry. The DAD (1104–1164) was placed in the sample cell at a concentration of $35 \mu\text{M}$ and thermostated to 25°C . Injections of the 10-fold higher concentrated FH3 domain led to an exothermic interaction that resulted in a dissociation constant K_d of $1.4 \mu\text{M}$ (Fig. 4A). The contribution of the enthalpy change ΔH of about $-4.9 \text{ kcal mol}^{-1}$ was combined with a highly favorable temperature-dependent change in entropy ($T\Delta S$) of $3.1 \text{ kcal mol}^{-1}$ to result in a change of free energy ΔG of $-8.0 \text{ kcal mol}^{-1}$. Mutation of the two DAD consensus motifs D2A and R5A revealed different contributions of the two signal sequences. While mutation of the positively charged cluster to alanine (R5A) slightly reduced the binding affinity (K_d $5.6 \mu\text{M}$) the hydrophobic patch MDLLV seemed to be necessarily required for the interaction. Here, mutation to alanine (D2A) significantly changed the shape of the heat disposal, which did not allow a straight fit. However, measurements of the same mutant at 15°C resulted in binding affinities around K_d $40 \mu\text{M}$. No binding could be detected for a DAD with simultaneous mutation of both motifs (DR9); the affinity of this peptide to the FH3 domain was too weak for ITC measurements. As control the FH3 domain was injected into the sample cell filled with buffer which showed no heat detachment. Measurements at 15°C resulted in similar binding affinities. The purity and integrity of the proteins used for ITC experiments is shown by Coomassie-stained SDS-PAGE (Fig. 4B). Interestingly, mutation of the positive charges led to slightly faster migration through the SDS gel (lane 3), while mutation of the hydrophobic DAD consensus motif (lane 4) led to delayed migration, suggesting the loss of structural conformation. Finally, comparable binding results were obtained when these DAD mutants were analyzed for *in vitro* binding to the FH3 domain (Fig. 4C). GST-fused FHOD1-DAD proteins were used to precipitate the FH3 domain from solution and bound proteins were stained with anti-His antibody. Thus, the MDLLV motif is the critical determinant for the autoregulatory interaction of FHOD1 *in vitro* and *in vivo*, and the basic cluster facilitates this binding.

Molecular Dispersion of the FH3-DAD Complex—We next intended to analyze the complex formation of the two molecules by size exclusion

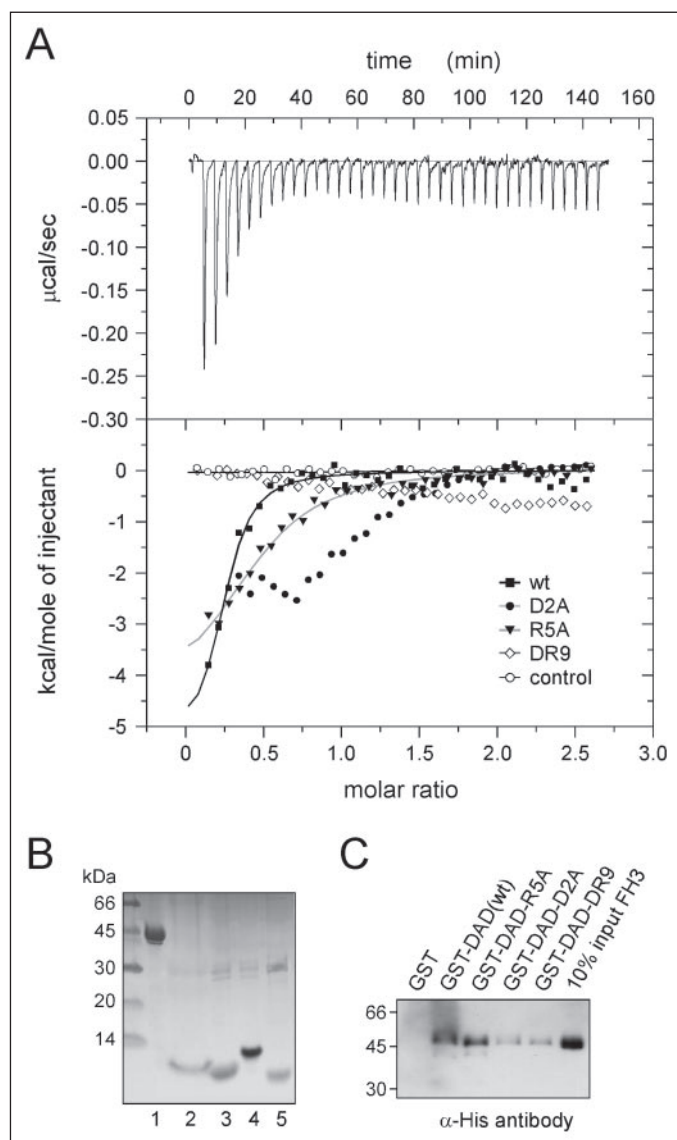


FIGURE 4. Binding affinities between of the DAD and its recognition domain. *A*, isothermal titration calorimetry of FHOD1 (1–377) with the DAD (1104–1164) revealed a dissociation constant of $1.4 \mu\text{M}$ for the wild type protein interaction. Mutation of the DAD consensus motifs MDLLV to AALAA (D2A) significantly changed the shape of the heat disposal, while mutation of the positive charged cluster RERKRSR to AEAASA (R5A) only slightly diminished the interaction. The double mutant (DR9) showed no binding. *B*, the proteins used for ITC experiments are shown by Coomassie-stained SDS-PAGE. The lanes correspond to the FH3 domain (1–377) (lane 1); DAD (wild type, 1104–1164) (lane 2), DAD-R5A (lane 3), DAD-D2A (lane 4), and DAD-DR9 (lane 5). *C*, *in vitro* precipitation of the FH3 domain by DAD proteins. Anti-His Western blot of a GST pull-down experiment with GST-fused DAD mutants and the N-terminal FHOD1 (1–377) domain.

chromatography to study the molecular dispersion and stoichiometry of their interaction. Several independent measurement cycles were performed on analytical gel filtration columns with different separation profiles. The Biosep column with an apparent cutoff of 300 kDa worked best and five representative chromatograms are shown in Fig. 5. For control, the elution contents were collected in fractions of 1 or 0.5 ml size and subjected to SDS-PAGE analysis. We first applied the FH3 domain (1–377) of FHOD1 in 50 mM Hepes buffer, pH 7.2, 100 mM NaCl, and 1 mM dithioerythritol. More than half of the protein appeared as dimer or trimer complex (elution time 12.97 min, calculated mass of 145 kDa), while the monomer fraction (14.57 min) showed a well defined elution profile that corresponded to a calculated mass of 46 kDa (Fig. 5, *top panel*). Under these buffer conditions, no higher mass aggre-

gates were formed. The DAD (1104–1164, apparent mass of 7.1 kDa) itself ran at an elution profile around 20 min (*second panel*). However, since the DAD itself contained no aromatic residues but one histidine within the linker segment that remained from the cloning site, this domain showed only little chromatographic absorption at 280 nm. Addition of the DAD to its FH3 recognition domain shifted the distribution toward the monomeric fraction and resulted in a slightly earlier elution time (14.47 min), while a minor peak at 12.92 min indicated the oligomeric complex (Fig. 5, *third panel*).

A different elution course of the molecules was observed when 10 mM dithioerythritol was added as reducing agent to the samples 30 min before application to the column (Fig. 5, *fourth and fifth panels*). Now, the FH3 domain remained mostly monomeric and only small peaks indicated oligomeric fractions. A similar behavior was observed upon addition of the even more reactive reducing agent TCEP (data not shown). The observations suggested that the formation of cysteine disulfide bonds may have led to the oligomer fraction. The elution profiles of the analytical gel filtrations are followed similarly in the individual fractions by SDS-PAGE analysis (*right panels*). The complex formation is indicated by a faint band of the DAD in the Coomassie-stained gels at the 14-ml fractions.

The small shift toward higher masses for the FH3·DAD complex (14.45 min) compared with the FH3 domain alone (14.56 min) indicated only a small increase in the overall molecular size. While the rather early elution time of the DAD alone may result from an elongated or partly flexible structure, the relatively small shift of the elution time for the complex indicated an only small increase in the overall size of the complex. This observation would be in line with a DAD peptide conformation that stretches over a globular folded FH3 recognition domain.

Mapping of the DAD-binding Interface by NMR Spectroscopy—Finally we set out to characterize the DAD binding interface to the FH3 domain by NMR spectroscopy. As proved first by ^1H NMR experiments, the 42-kDa FH3 domain was highly soluble and stable and could be concentrated up to 0.7 mM in aqueous buffer without any indication for aggregation. The chemical shift distribution of NH and C_αH resonances suggested an all helical fold for the 377-residue domain (data not shown). The recombinantly expressed DAD of 61 amino acid length (1104–1164) was soluble up to 0.6 mM in phosphate buffer but appeared rather unstable and was partially degraded after 2 days measurement time at 25 °C.

We next used uniformly ^{15}N -labeled DAD protein to measure a titration series with its recognition domain by $^1\text{H}/^{15}\text{N}$ HSQC experiments (Fig. 6A). The peak distribution of the uncomplexed DAD (*blue signals*) suggested an intrinsically unstructured protein domain. The ^{15}N resonance signals largely reflected random coil chemical shift positions, while some high field shifted ^1H chemical shifts (7.7–8.0 ppm) would indicate a tendency for an α -helical content. We assigned the resonance signals using correlation spin systems and sequential NOE path. Interestingly, residues within the hydrophobic DAD consensus motif showed highfield shifted resonances and stronger sequential $\text{H}^{\text{N}}\text{-H}^{\text{N}}$ NOE correlations indicating a helical conformation for this region (Fig. 6B).

Titration of the FH3 domain (1–377) was achieved in three steps with molar ratios of 0.3, 0.6, and 1.1 (FH3 to DAD) by addition of the FH3 domain from 0.7 mM stock solution to the DAD and subsequent concentration. During binding saturation more than half of the 67 DAD resonance signals disappeared indicating the interaction with the FH3 domain, while about 30 $^1\text{H}/^{15}\text{N}$ backbone signals remained visible (*red signals*). This suggested that the directly interacting residues of the DAD adopted the diffusion behavior of the receiving FH3 molecule, while the

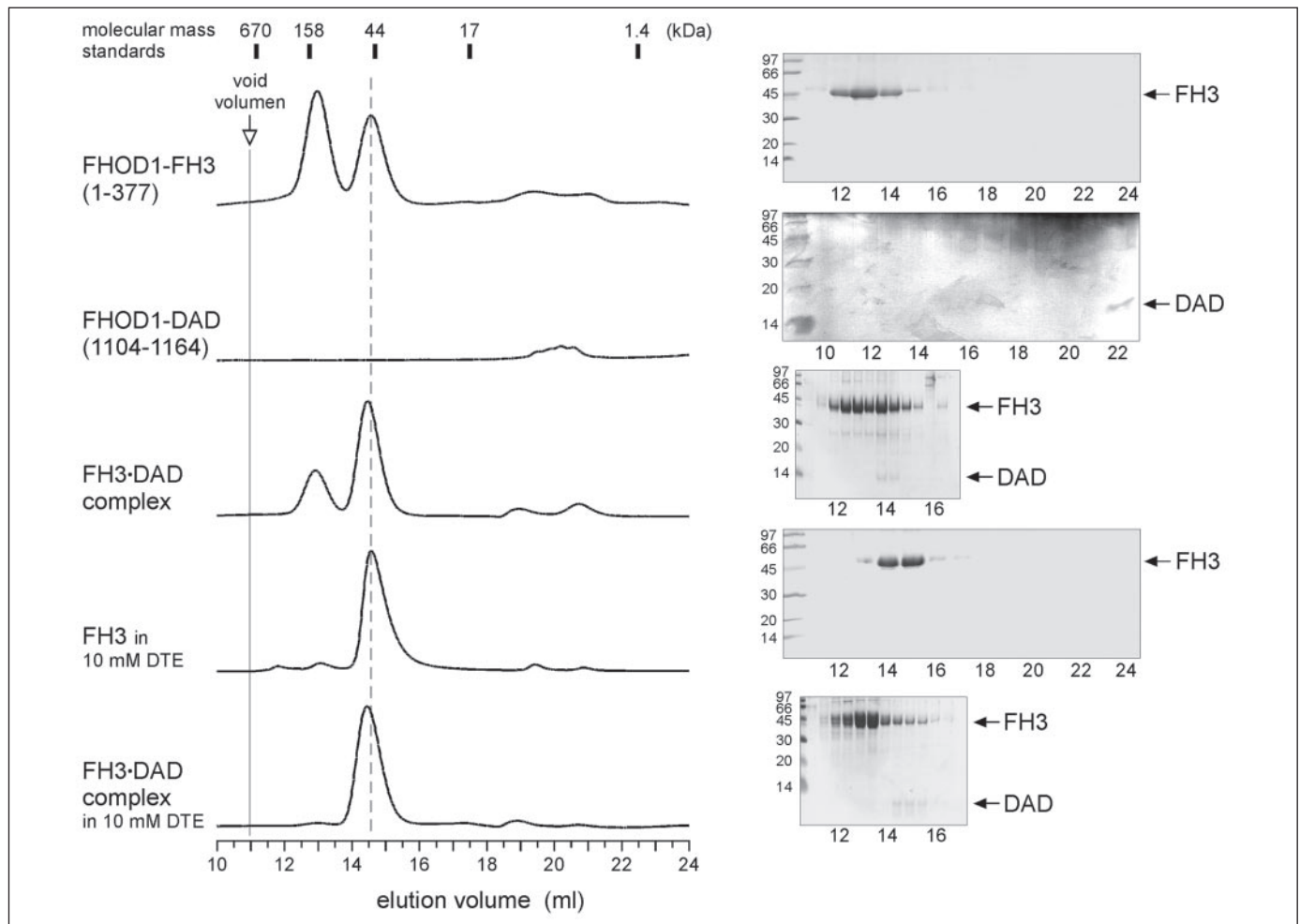


FIGURE 5. Molecular dispersion of the FH3-DAD complex. Proteins were eluted in 50 mM Hepes, pH 7.2, 100 mM NaCl, and 1 mM dithioerythritol buffer. The elution contents were collected in fractions of 1 or 0.5 ml size and monitored by 17% SDS-PAGE analysis on the right hand site. *Upper panel*, size exclusion chromatography of the FH3 domain (1–377) alone indicated a monomer-dimer distribution. *Second panel*, the 60-residue DAD (1104–1164) eluted late from the column and showed only minor absorption due to the lack of aromatic residues. Elution of the diluted protein was verified by silver staining. *Third panel*, addition of the DAD to the FH3 domain led to a decreased multimerization, and the small shift in size indicated the complex formation. *Fourth and fifth panels*, addition of 10 mM dithioerythritol to the samples prior to application to the column resulted in monomerization of the proteins. The small shift toward earlier elution times for the FH3-DAD samples (compare *gray dashed line*) suggests only a small increase for the overall molecular size of the complex. SDS-PAGE analysis of the elution fractions shown on the *right* confirmed the integrity of the proteins and the formation of the complexes.

non-interacting residues remained largely flexible, since the chemical shift positions of these residues did not vary. Moreover, we find that all but one glycine residue remained unchanged upon complexation, while most resonance signals typically assigned to serine or threonine residues disappeared. This resulted in a mapping of the binding interface of the DAD to the FH3 domain to about 40 residues from Asp¹¹⁰⁵ to Ser¹¹⁴⁴ including both the hydrophobic and charged DAD consensus motifs (Fig. 6C). In line with the previous protein interaction results, our observations suggest that the DAD acts as an unstructured domain composed of two individual signal sequences rather than a structural domain with a well folded binding interface.

DISCUSSION

The data presented here demonstrate that the C-terminal 60 amino acids of FHOD1 form its DAD that interacts as an intrinsically unstructured signal sequence with the N-terminal 377 residues, which forms the FH3 domain. These observations are surprising by two means. First, the DAD recognition site differs from the proposed GTPase-binding domain in FHOD1 (16). This questions the mechanism of activation for FHOD1, since in other DRFs the competition between the inhibitory DAD, and the activating GTPase for a mutually exclusive binding site is

believed to stimulate conformational changes in the formin that subsequently lead to unmasking of the actin-nucleating FH1-FH2 module. Second, the DAD in FHOD1 appears of smaller size than expected, since one of the proposed hydrophobic DAD consensus motifs turned out not to be required for autoregulation. This implies that either the FH2 domain in FHOD1 is considerably longer than in other Dia-family proteins or that FHOD1 contains an additional module of yet unknown function in between the FH2 domain and the DAD (see Fig. 1D, *right panel*).

While the FH1 and FH2 domains share significant sequential homology in formin proteins of all different species, sequence homology within the DADs that constitute the DRF family is limited to a hydrophobic MDxLL signal motif and a basic cluster of at least five residues (Fig. 1). Since FHOD1 contains two hydrophobic signal motifs and one basic cluster, we first analyzed by *in vitro* binding experiments and functional *in vivo* transfections the individual relevance of the three motifs (Figs. 2 and 3). As clearly shown, the first motif at position 1053 did not contribute to the binding of the DAD to its N-terminal recognition domain and mutation to alanine in the full-length protein did not induce biological activities of FHOD1. In contrast, mutation of the second motif MDxLV at position 1108 to alanine significantly increased

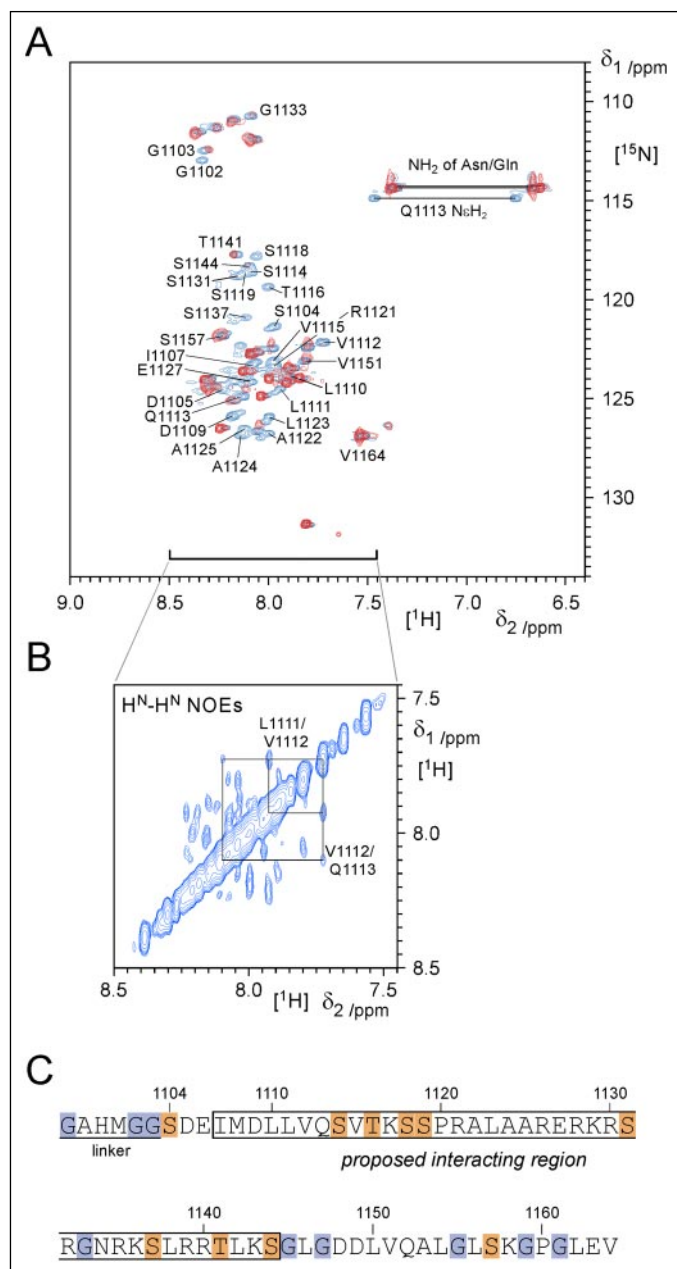


FIGURE 6. NMR analysis of the DAD-FH3 domain interaction. *A*, overlay of $^1\text{H}/^{15}\text{N}$ HSQC spectra of ^{15}N -labeled DAD alone (blue) and in complex with the FH3 domain (red). While the DAD appeared initially largely unfolded, about half of the resonance signals disappeared upon complexation with its FH3 recognition domain. This suggested the induction of a folded binding interface for the interacting residues, whereas the remaining residues stay unstructured and flexible. Residues that disappeared upon binding are indicated. Spectra were recorded in 20 mM KP_i, pH 7.2, 50 mM NaCl, 1 mM TCEP at 25 °C. *B*, ^1H - ^1H region of a two-dimensional NOESY spectrum of the DAD. The chemical shift change and the increased NOE correlations indicate a helical conformation for the hydrophobic DAD consensus motif as mapped for V1112. *C*, delineation of glycine, serine, and threonine residues to the protein sequence of the DAD. The disappearance or remaining of resonance signals suggested a mapping of the binding interface of the DAD to the FH3 domain to a central region of ~40 residues.

actin stress fiber formation and SRE transcription and the positively charged cluster additionally contributed to a minor extend to this phenotype. These observations correlated with the binding affinities between the DAD or mutants thereof and the N-terminal recognition domain as determined by isothermal titration calorimetry (Fig. 4).

We next asked whether these conserved motifs form the scaffold of the autoregulation domain or if they act themselves as signal sequences.

NMR experiments of heteronuclear labeled DAD revealed that the 61-residue fragment of FHOD1 does not appear as a folded domain but rather seems to be intrinsically unstructured with some helical content (Fig. 6). Indeed, mapping of the binding interface derived from titration experiments with the FH3 domain suggested that a region (1106–1144) including both motifs is involved in the interaction, while residues at the far C terminus remained flexible and unperturbed. Thus, the defining DAD consensus motifs rather act as signal sequences for binding to their recognition sites. In support of the NMR experiments, analytical gel filtration revealed that complex formation of the DAD to the FH3 domain only slightly increased the globular size of the complex (Fig. 5). This may suggest an interaction similar to the binding between β -catenin and E-cadherin, where a long unstructured fragment of E-cadherin is stretched out over the extended repeat structure of β -catenin (38).

Our functional analysis of FHOD1 variants in NIH3T3 cells provided several new insights in the formation of actin stress fibers by the activated DRF. A rough correlation was observed between the ability of FHOD1 to induce actin stress fibers and to enhance SRE transcription. These results are consistent with previous observations made for other DRFs (13, 30, 39, 40). However, FHOD1-R5A was moderately active in stress fiber formation but failed to trigger SRE transcription. This might reflect that threshold levels of actin polymerization must be reached to efficiently induce serum response factor activity. For mDia1, the correlation between stress fiber formation and SRE activity reflects the control of nuclear import of the serum response factor coactivator MAL by cytoplasmic actin treadmilling (41, 42). Whether the same mechanism applies to FHOD1-induced SRE activation warrants future investigation. Importantly, stress fiber formation by FHOD1/2 was previously only described upon experimental truncation of the protein (17, 18, 20, 37). Data presented here now demonstrate that this activity is also observed in the context of the full-length protein upon release of autoinhibition, supporting a putative physiological relevance of the actin stress fiber phenotype. Interestingly, the stress fiber morphology differed between the various FHOD1 variants analyzed. While the partially activated FHOD1 D2A variant only induced thin actin filaments, FHOD1 DR9 triggered bundling of these filaments into thicker fibers. This suggests that a stepwise regulation of FHOD1 autoinhibition may yield FHOD1 proteins with distinct biological properties. Of note, FHOD1 DR9 induced thick actin bundles without appreciable association with these filaments. This finding excludes previous speculations that the unique architecture of thick stress fibers induced by FHOD1- ΔC reflects its ability to stably decorate these structures (43). Rather, intrinsic differences in the employed molecular mechanisms and regulation of FHOD1 relative to other DRFs must account for its ability to create thick F-actin bundles.

The discrepancy in the targeting of two distinct domains for autoregulation (via the DAD-FH3 (1–377) interaction) and activation (via the Rac1-GBD (411–573) interaction) requires further investigation. Recent crystallographic studies of the mouse mDia1 protein have elucidated the structure of a N-terminal GTP-binding/FH3 domain followed by a dimerization region from residue 83 to 474 (31, 32). Further NMR mapping experiments and fluorescence titrations suggested similar binding surfaces for the two regulating molecules. In this scenario, release of autoinhibition leading to DRF activation can easily be envisioned as consequence of competitive binding. But how could autoregulation be released in FHOD1? We tested a putative interaction between the FH3 domain and the proposed GBD; however, no binding of the two domains could be observed (data not shown) that might induce a mutually exclusive interaction, e.g. by steric hindrance. Alternatively, other yet unknown cofactors could be implied for the activa-

tion in cells. Such effectors might strengthen the interaction with Rac1. Additionally, they could select for the activation status of the GTPase and/or facilitate the release of the autoinhibitory FH3-DAD interaction upon interaction with Rac1. The identification of such factors will represent an important task for future studies toward the understanding of the physiological role and molecular regulation of this DRF. Finally, also the exact boundaries of the Rac1 interaction site in FHOD1 should be reinvestigated and carefully characterized biochemically. Based on our molecular characterization of the autoregulation in FHOD1, future studies will be directed toward the structural understanding of this interaction.

Acknowledgments—We thank Friederike Vollmuth for initial cloning and expression studies of the DAD, Diana Ludwig and Santiago Manrique for expert technical assistance, and Bernhard Griewel for expert assistance with NMR measurements. M. G. and O. T. F. kindly acknowledge continuous support from Roger S. Goody and Hans-Georg Kräusslich.

REFERENCES

- Waller, B. J., and Alberts, A. S. (2003) *Trends Cell Biol.* **13**, 435–446
- Tanaka, K. (2000) *Biochem. Biophys. Res. Commun.* **267**, 479–481
- Zigmond, S. H. (2004) *Curr. Opin. Cell Biol.* **16**, 99–105
- Watanabe, N., and Higashida, C. (2004) *Exp. Cell Res.* **301**, 16–22
- Pring, M., Evangelista, M., Boone, C., Yang, C., and Zigmond, S. H. (2003) *Biochemistry* **42**, 486–496
- Sagot, I., Rodal, A. A., Moseley, J., Goode, B. L., and Pellman, D. (2002) *Nat. Cell Biol.* **4**, 626–631
- Pruyne, D., Evangelista, M., Yang, C., Bi, E., Zigmond, S., Bretscher, A., and Boone, C. (2002) *Science* **297**, 612–615
- Alberts, A. S. (2001) *J. Biol. Chem.* **276**, 2824–2830
- Gasman, S., Kalaidzidis, Y., and Zerial, M. (2003) *Nat. Cell Biol.* **5**, 195–204
- Kohno, H., Tanaka, K., Mino, A., Umikawa, M., Imamura, H., Fujiwara, T., Fujita, Y., Hotta, K., Qadota, H., Watanabe, T., Ohya, Y., and Takai, Y. (1996) *EMBO J.* **15**, 6060–6068
- Evangelista, M., Blundell, K., Longtine, M. S., Chow, C. J., Adames, N., Pringle, J. R., Peter, M., and Boone, C. (1997) *Science* **276**, 118–122
- Habas, R., Kato, Y., and He, X. (2001) *Cell* **107**, 843–854
- Tominaga, T., Sahai, E., Chardin, P., McCormick, F., Courtneidge, S. A., and Alberts, A. S. (2000) *Mol. Cell* **5**, 13–25
- Higgs, H. N., and Peterson, K. J. (2005) *Mol. Biol. Cell* **16**, 1–13
- Westendorf, J. J., Mernaugh, R., and Hiebert, S. W. (1999) *Gene (Amst.)* **232**, 173–182
- Westendorf, J. J. (2001) *J. Biol. Chem.* **276**, 46453–46459
- Gasteier, J. E., Madrid, R., Krautkramer, E., Schroder, S., Muranyi, W., Benichou, S., and Fackler, O. T. (2003) *J. Biol. Chem.* **278**, 38902–38912
- Koka, S., Neudauer, C. L., Li, X., Lewis, R. E., McCarthy, J. B., and Westendorf, J. J. (2003) *J. Cell Sci.* **116**, 1745–1755
- Gasteier, J. E., Schroeder, S., Muranyi, W., Madrid, R., Benichou, S., and Fackler, O. T. (2005) *Exp. Cell Res.* **306**, 192–202
- Kanaya, H., Takeya, R., Takeuchi, K., Watanabe, N., Jing, N., and Sumimoto, H. (2005) *Genes Cells* **10**, 665–678
- Moseley, J. B., Sagot, I., Manning, A. L., Xu, Y., Eck, M. J., Pellman, D., and Goode, B. L. (2004) *Mol. Biol. Cell* **15**, 896–907
- Higashida, C., Miyoshi, T., Fujita, A., Ocegüera-Yanez, F., Monypenny, J., Andou, Y., Narumiya, S., and Watanabe, N. (2004) *Science* **303**, 2007–2010
- Romero, S., Le Clairche, C., Didry, D., Egile, C., Pantaloni, D., and Carlier, M. F. (2004) *Cell* **119**, 419–429
- Shimada, A., Nyitrai, M., Vetter, I. R., Kuhlmann, D., Bugyi, B., Narumiya, S., Geeves, M. A., and Wittinghofer, A. (2004) *Mol. Cell* **13**, 511–522
- Xu, Y., Moseley, J. B., Sagot, I., Poy, F., Pellman, D., Goode, B. L., and Eck, M. J. (2004) *Cell* **116**, 711–723
- Otomo, T., Tomchick, D. R., Otomo, C., Panchal, S. C., Machius, M., and Rosen, M. K. (2005) *Nature* **433**, 488–494
- Watanabe, N., Kato, T., Fujita, A., Ishizaki, T., and Narumiya, S. (1999) *Nat. Cell Biol.* **1**, 136–143
- Li, F., and Higgs, H. N. (2003) *Curr. Biol.* **13**, 1335–1340
- Li, F., and Higgs, H. N. (2005) *J. Biol. Chem.* **280**, 6986–6992
- Copeland, J. W., and Treisman, R. (2002) *Mol. Biol. Cell* **13**, 4088–4099
- Rose, R., Weyand, M., Lammers, M., Ishizaki, T., Ahmadian, M. R., and Wittinghofer, A. (2005) *Nature* **435**, 513–518
- Otomo, T., Otomo, C., Tomchick, D. R., Machius, M., and Rosen, M. K. (2005) *Mol. Cell* **18**, 273–281
- Petersen, J., Nielsen, O., Egel, R., and Hagan, I. M. (1998) *J. Cell Biol.* **141**, 1217–1228
- Schulte, A., Czudnochowski, N., Barboric, M., Schonichen, A., Blazek, D., Peterlin, B. M., and Geyer, M. (2005) *J. Biol. Chem.* **280**, 24968–24977
- Neidig, K. P., Geyer, M., Gorler, A., Antz, C., Saffrich, R., Beneicke, W., and Kalbitzer, H. R. (1995) *J. Biomol. NMR* **6**, 255–270
- Geyer, M., Munte, C. E., Schorr, J., Kellner, R., and Kalbitzer, H. R. (1999) *J. Mol. Biol.* **289**, 123–138
- Takeya, R., and Sumimoto, H. (2003) *J. Cell Sci.* **116**, 4567–4575
- Huber, A. H., and Weis, W. I. (2001) *Cell* **105**, 391–402
- Copeland, J. W., Copeland, S. J., and Treisman, R. (2004) *J. Biol. Chem.* **279**, 50250–50256
- Sotiropoulos, A., Gineitis, D., Copeland, J., and Treisman, R. (1999) *Cell* **98**, 159–169
- Posern, G., Sotiropoulos, A., and Treisman, R. (2002) *Mol. Biol. Cell* **13**, 4167–4178
- Miralles, F., Posern, G., Zaromytidou, A. I., and Treisman, R. (2003) *Cell* **113**, 329–342
- Madrid, R., Gasteier, J. E., Bouchet, J., Schroder, S., Geyer, M., Benichou, S., and Fackler, O. T. (2005) *FEBS Lett.* **579**, 441–448